# *Ab initio* modeling of the motional Stark effect on MAST[a)]

M. F. M. De Bock,[b)] N. J. Conway, M. J. Walsh, P. G. Carolan, and N. C. Hawkes
*EURATOM/UKAEA Fusion Association, Culham Science Centre, Abingdon OX14 3DB, United Kingdom*

(Presented 15 May 2008; received 9 May 2008; accepted 14 July 2008; published online 31 October 2008)

A multichord motional Stark effect (MSE) system has recently been built on the MAST tokamak. In MAST the $\pi$ and $\sigma$ lines of the MSE spectrum overlap due to the low magnetic field typical for present day spherical tokamaks. Also, the field curvature results in a large change in the pitch angle over the observation volume. The measured polarization angle does not relate to one local pitch angle but to an integration over all pitch angles in the observation volume. The velocity distribution of the neutral beam further complicates the measurement. To take into account volume effects and velocity distribution, an *ab initio* code was written that simulates the MSE spectrum on MAST. The code is modular and can easily be adjusted for other tokamaks. The code returns the intensity, polarized fraction, and polarization angle as a function of wavelength. Results of the code are presented, showing the effect on depolarization and wavelength dependence of the polarization angle. The code is used to optimize the design and calibration of the MSE diagnostic. © *2008 American Institute of Physics.* [DOI: 10.1063/1.2966459]

## I. INTRODUCTION

Motional Stark effect (MSE) diagnostics are used in tokamaks to measure the pitch angle of the magnetic field, from which the poloidal magnetic field and the current distribution can be deduced.[1] A MSE diagnostic analyzes the light emitted by neutral beam particles—in the case of the MAST tokamak this is $D_\alpha$ emission. Due to the neutral particle velocity $\boldsymbol{v}$, with respect to the magnetic field $\boldsymbol{B}$, the particle experiences a Lorentz electric field $\boldsymbol{E}_l=\boldsymbol{v}\times\boldsymbol{B}$. Together with the electrostatic field $\boldsymbol{E}_s$, this yields a total electric field $\boldsymbol{E}=\boldsymbol{E}_l+\boldsymbol{E}_s$ that causes degenerate energy levels of the neutral beam particles to split up, with multiple emitted transition lines as a result. The transition lines can be divided in two groups: $\pi$ and $\sigma$, that emit light polarized parallel and perpendicular to the electric field, respectively. Examining the polarization of the emitted $\pi$ or $\sigma$ light thus reveals the angle of the electric field and consequently the pitch angle of the magnetic field (assuming $\boldsymbol{v}$ and $\boldsymbol{E}_s$ are known).

After the successful testing of a pilot diagnostic,[2] work commenced on a full-scale, multichord MSE diagnostic for MAST. As part of the development of the multichord MSE diagnostic, a modeling code was written that calculates the full MSE spectrum. This means not only the intensity $I$ but also polarization angle $\gamma$ and linear polarization fraction $p_l$ are returned as function of wavelength ($\lambda$). Because of the low magnetic field in MAST, the Stark splitting is small. The broadening of the spectrum, both due to the variation in $\boldsymbol{E}_s$ and $\boldsymbol{B}$ within the collection volume and Doppler broadening, due to the beam velocity distribution and the finite collection solid angle, is larger than the Stark splitting, causing a strong overlap of the $\pi$ and $\sigma$ lines. The overlap of emission lines with a difference in local polarization angles close to 90° causes significant depolarization and influences the observed overall polarization angle.

To describe the MSE physics as accurately as possible, the modeling code presented here starts from first principles. It incorporates the three dimensional (3D) nature of the physics, taking into account the variation of $\boldsymbol{B}$, $\boldsymbol{E}_s$, beam emission, and beam velocity distribution over the collection volume (i.e., the intersection of the viewing cone and the neutral beam). The beam velocity distribution is treated as a five dimensional function providing at each spatial point the probability that a beam particle moves with a horizontal and a vertical angle with respect to the beam axis. Finally the simulation code also incorporates the two dimensional (2D) solid angle of the collection optics and the effect of the narrow bandpass filter used to select the $\pi$ or $\sigma$ component of the spectrum. For a correct propagation of the total polarization state—intensity $I$, polarization angle $\gamma$, and fraction $p_l$—through the integration, Stokes vectors are used. The atomic physics—i.e., the normalized intensities of the different $\pi$ and $\sigma$ lines and the linear, quadratic, and cubic Stark wavelength shift factors—is treated by an independent module in the code, such that more complex atomic processes, such as dynamic population of Stark levels due to comparable $l$ mixing and de-excitation lengths can, in principle, be modeled readily.[3,4] So far, however, only a statistical population of the Stark levels has been used. Not yet implemented in the code is the Zeeman effect that would cause some circular polarizations and is usually assumed to be small, and polarized emission due to reneutralized fast ions.[5]

The code assisted the design of the new system and allows to quantify and correct for systematic errors arising from, e.g., the beam velocity distribution and finite collection

[a)]Contributed paper, published as part of the Proceedings of the 17th Topical Conference on High-Temperature Plasma Diagnostics, Albuquerque, New Mexico, May 2008.

[b)]Electronic mail: maarten.de.bock@ukaea.org.uk. URL: http://www.fusion.org.uk/.

 

volume. Furthermore, it provides a better understanding of the measured signals and it can be used as a forward function in the Bayesian equilibrium reconstruction.[6] Because the effects of finite volume and velocity distribution are not unique to MAST, the code was written in a machine-independent way so that it can be used as a MSE tool for other plasma devices as well.

In Sec. II the modeling code is described. Section III presents some of the results of the code. Finally, Sec. VI gives a brief overview of the recently installed multichord MSE system on MAST.

## II. DESCRIPTION OF THE MODEL

The code performs an integration over seven dimensions: the collection volume (3D) and solid angle (2D), and the velocity distribution of the beam particles with respect to the beam axis (2D). A separate routine performs a final integration over wavelength, taking into account the narrow bandpass filter that selects the $\pi$ or $\sigma$ component of the spectrum.

All machine-dependent properties are described in the setting files, not in the routines, making it possible to run the code for other devices than MAST.

The magnetic field configuration, the neutral beam emission profile, and velocity distribution can be provided by any beam and/or equilibrium code. Also the atomic physics data—normalized intensities and wavelength shift factors—are provided separately.

The code was developed from an earlier code written by Carolan.[7]

### A. Finite observation volume

The 3D spatial integration grid should cover the collection volume as accurately as possible. The modeling code uses a set of integration points that resembles the image of the fiber bundle—for each channel—at the position of the neutral beam. Usually the distance between the collection lens and the neutral beam is much larger than the distance between the fibers and the lens so the image of a fiber at the position of the neutral beam can be seen as a cylinder. The diameter of the cylinder is determined by the fiber diameter and the magnification of the collection optics. The length of this cylinder is chosen such that it covers the complete path through the neutral beam. Finally, each cylinder is divided in a number of slices to form a grid of integration points (the center of each slice) and volumes.

### B. Equilibrium and neutral beam models

The magnetic field configuration and the intensity of the $D_\alpha$ emission of the neutral beam are calculated by separate codes.[8,9] Because the measured polarization angle depends on the beam velocity, the beam model should also include the velocity distribution of the neutral beam particles. This beam velocity distribution depends on the geometric focusing of the beamlets in the beam source and the divergence of each beamlet. In Fig. 1(a) a simple beam source is sketched with three beamlets focused at point $f$. We assume the brightness of all beamlets to be equal and the

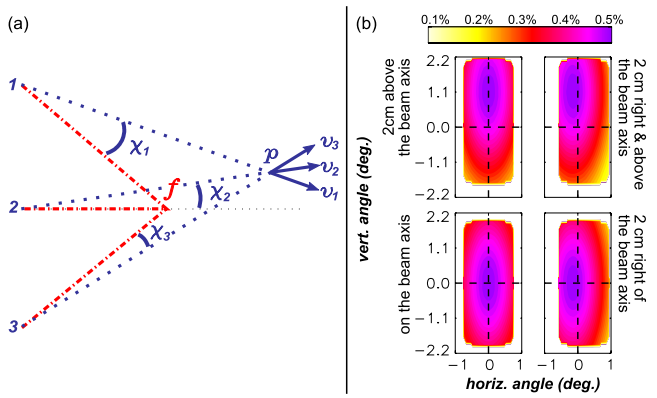


FIG. 1. (Color online) (a) Velocity distribution at point $p$ for three beamlets with a focus at point $f$. (b) MAST velocity distribution for four spatial points around and on the beam axis at $R=1.10$ m (probability: maximum of 0.5%, minimum of 0.1%, sum over all 262 beamlets: 100%).

divergence distribution given by $1/(\xi\sqrt{\pi})\exp(-\chi^2/\xi^2)$, with $\chi$ the divergence angle and $\xi$ the half $1/e$ width. A beam particle arriving at an arbitrary point $p$ can only have three possible directions, given by $\boldsymbol{v}_1$, $\boldsymbol{v}_2$, and $\boldsymbol{v}_3$. The probability $P_x$ that a the particle moves in direction $\boldsymbol{v}_x$ is $P_x = \exp(-\chi_x^2/\xi^2)/\Sigma_{i=1}^3[\exp(-\chi_i^2/\xi^2)]$.

The velocity distribution is a five dimensional function returning at each spatial point $p(x,y,z)$, the probability that a beam particle moves with horizontal and vertical angles with respect to the beam axis. In Fig. 1(b) the velocity distribution of the MAST south PINI is given as a function of horizontal and vertical angle for four spatial points around and on the beam axis at major radius $R=1.1$ m (approximately equal to half minor radius in MAST). The MAST PINI source has 262 beamlets, each having a Gaussian divergence distribution with a half $1/e$ width of 0.7°, with a vertical focus located at 5.17 m from the beam source and a horizontal focus at 14.0 m.[10] One observes that the geometrical focusing has a severe effect on the velocity distribution, especially with respect to the vertical angle. Also the velocity distribution shows a significant variation with position.

### C. Calculation of the MSE spectrum

For each emission element—determined by the spatial point, emission direction, and beam velocity vector—the simulation code determines the wavelengths λ of the $\pi$ and $\sigma$ emission lines by calculating the Doppler and Stark shifts. Subsequently Stokes vectors are calculated as a function of λ. The Stokes vector describes the polarization state of the emitted light: $S(I,\gamma,p_l,p_c)=[I,p_lI\cos(2\gamma),p_lI\sin(2\gamma),p_cI]$, with $I$ the total intensity, $\gamma$ the polarization angle, $p_l$ the linear polarization fraction, and $p_c$ the circular polarization fraction. To find the total polarization state of the sum of several light sources one just adds up the Stokes vectors. For two linearly polarized light sources $S_{\text{total}}(I,\gamma,p_l,p_c) = S_1(I_1,0,1,0)+S_2(I_2,\delta\gamma,1,0)$, one gets

$$\gamma = \frac{1}{2}\tan^{-1}\left[\frac{\sin(2\delta\gamma)}{I_1/I_2+\cos(2\delta\gamma)}\right], \tag{1}$$

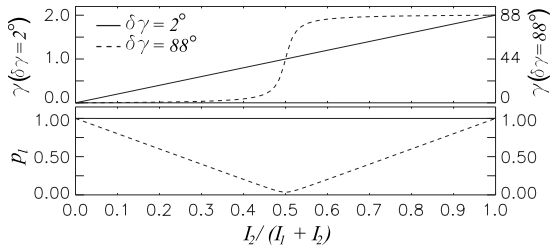


FIG. 2. $\gamma$ and $p_l$ as function of the intensity ratio of two polarized emission sources: one at 0° and one at $\delta\gamma$.

$$p_l = \frac{\sqrt{[I_1/I_2 + \cos(2\delta\gamma)]^2 + \sin^2(2\delta\gamma)}}{1 + I_1/I2}. \quad (2)$$

In Fig. 2 $\gamma$ and $p_l$ are plotted as a function of $I_2/(I_1+I_2)$ for $\delta\gamma=2°$ and $\delta\gamma=88°$. For small $\delta\gamma$, $\gamma$ changes almost linearly between 0° and $\delta\gamma$ when the intensity ratio goes from full $I_1$ to full $I_2$. The polarization fraction remains close to 100%. For $\delta\gamma$ close to 90°, however, $\gamma$ resembles a step function with a very strong variation in $\gamma$ for a small change in the intensity ratio around $I_1=I_2$. Also the polarization fraction shows a large reduction.

The latter is important in low $B_\phi$ devices such as MAST. Due to the overlap of $\pi$ and $\sigma$ components, Stokes vectors with a difference in polarization angle around 90° are summed up, resulting in significant depolarization and possibly large variations in the overall polarization angle.

With the Stokes vectors as function of λ known for each emission element, those at the same wavelength are added up to obtain the total Stokes vector as a function of λ. Finally the narrow bandpass interference filter is applied by multiplying the total Stokes vector by the filter transmission function and integrating over the wavelength. The resulting Stokes vector gives the intensity $I$, the polarization angle $\gamma$, and the polarization fraction $p_l$ as a function of the central wavelength of the narrow bandpass filter ($\lambda_{CWL}$).

$$S_{total}(\lambda_{CWL}) = \int_{\lambda_{min}}^{\lambda_{max}} \text{filter}(\lambda - \lambda_{CWL}) \int_{V_{coll.}} \int_{\Omega_{coll.}} \int_{\boldsymbol{v}_{beam}} \times S_{local}(\lambda) dV d\Omega dv_{beam} d\lambda, \quad (3)$$

with $V_{coll.}$ the collection volume, $\Omega_{coll.}$ the collection solid angle, and $\boldsymbol{v}_{beam}$ the beam velocity vectors.

## III. RESULTS

The beam and equilibrium models used in the simulations shown below were calculated based on MAST discharge 18501 at $t=0.29$ s. The plasma current was 0.75 MA, the central electron density was $3.5\times10^{19}$ m$^{-3}$, the central electron temperature was 1.4 keV, and the voltage of the deuterium neutral beam was 63 kV. Equilibrium FIT (Ref. 9) was used for the equilibrium construction and the beam was modeled with a code by Turnyanskiy,[8] that uses atomic data and analysis structure (ADAS) for the ionization and emission rate coefficients.[11]

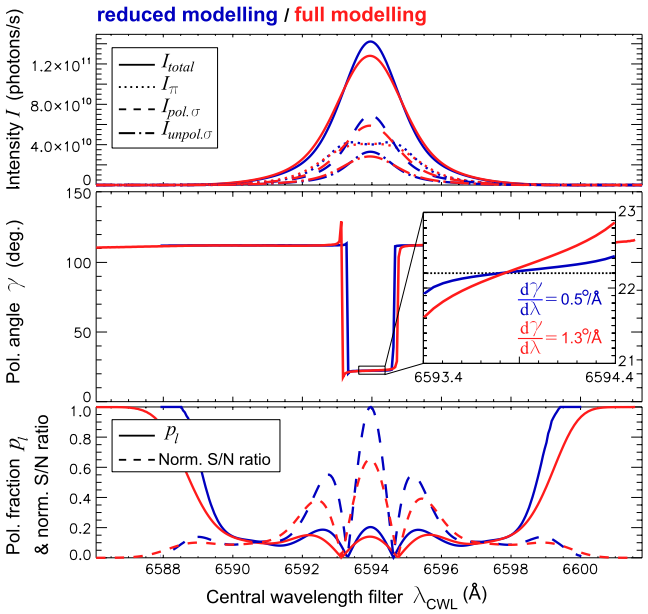


FIG. 3. (Color online) Comparison between reduced and full modeling of the Stark spectrum. The spectra shown were calculated for a channel at $R=1.36$ m.

### A. Reduced versus full modeling

One could question whether full modeling, which requires a long calculation time, is really necessary. A comparison was therefore made between a reduced and full model, both applied for the same viewing geometry (channel 27 at $R=1.36$ m in midplane geometry, see below). In the reduced model only one spatial point (on the beam axis) is sampled and the beam velocity distribution is set to a $\delta$ function on the beam axis. The integration over the finite solid angle of the collection optics is retained. To both simulated spectra a narrow bandpass filter [full width at half maximum (FWHM) 1.2 Å] was applied.

The result is shown in Fig. 3, where $I$, $\gamma$, $p_l$, and the normalized signal to noise (S/N) ratio are given as a function of the central wavelength of the interference filter ($\lambda_{CWL}$). The intensity spectrum is split up in its main components of polarized $\pi$ emission, polarized $\sigma$ emission, and unpolarized $\sigma$ emission. The unpolarized $\pi$ emission, that exists due to the overlap of $\pi$ emission with slightly different polarization angles, is very low and can be neglected. The normalized S/N ratio in the lower graph of Fig. 3 is proportional to $p_l\sqrt{I}$ because the useful signal is given by $p_l I$, while the (Poisson) noise is estimated from $\sqrt{I}$. It is normalized with respect to the maximum value of the two simulations (i.e., the S/N ratio of the reduced modeling at the peak of the spectrum).

One observes a clear difference between the reduced and full modeling. First of all the full modeling predicts a broader spectrum with less structure in the $\pi$ component of the spectrum than the reduced modeling. This can mainly be attributed to extra Doppler broadening caused by the beam velocity distribution. More important for the purposes of MSE, however, is the effect on the polarization angle and polarization fraction.

Compared to the reduced model, the full simulation shows a stronger dependence of the polarization angle on the

$\lambda_{CWL}$ ($d\gamma/d\lambda$). Full modeling predicts that an inaccuracy in $\lambda_{CWL}$ of 1 Å can result in a systematic error of 1.3° in the measured polarization angle. A reduced simulation would only predict a 0.5° deviation of the polarization angle for the same inaccuracy in $\lambda_{CWL}$. The fact that there is still a dependence of the polarization angle on $\lambda_{CWL}$ in a reduced simulation is due to the finite solid angle of the collection optics—responsible for a distribution of polarization angles—and the interference filter—which adds up different polarization angles at different wavelengths. Often this effect is ignored in MSE simulations and a $\lambda_{CWL}$-independent angle is given—i.e., assuming a zero solid angle for the collection optics and an infinitely narrow bandpass filter. This $\lambda_{CWL}$-independent polarization angle is given by the dotted line in the inset of the polarization angle plot. Also the full simulation predicts a lower polarization fraction than the reduced modeling: 13% versus 20% at the peak of the spectrum. As a result the predicted $S/N$ ratio is about 35% lower when using a full model than when using a reduced model.

The above shows that including a finite collection volume and an accurate beam velocity distribution has a significant effect on the simulated MSE spectra for MAST. Leaving them out would result in overly optimistic predictions of the statistic ($\propto p_l^{-1}$) and systematic ($\propto d\gamma/d\lambda$) errors. The full modeling is therefore essential when predictions are to be made on the expected performance of a multichord MSE diagnostic.

### B. Effect of viewing geometry and interference filter bandwidth

In designing a MSE diagnostic, there is a certain freedom of choice on the position of the collection optics, the layout of the fiber bundle, and the bandwidth of the interference filter. The 3D modeling code was used to assess the effect of changing these parameters on observables such as the spatial resolution of the diagnostic, the normalized S/N ratio (again normalized with respect to the maximum value of the two simulations), and the dependence of the measured polarization angle on $\lambda_{CWL}$ of the filter ($d\gamma/d\lambda$).

In Fig. 4 the spatial resolution, $d\gamma/d\lambda$, $p_l$, and the normalized S/N ratio—all at the peak of the spectrum—are shown for two viewing geometries. One of the viewing geometries—the top view—has its collection optics 0.45 m above the midplane of the tokamak such that its lines of sight look down on the neutral beam; the second viewing geometry—the midplane view—has its collection optics and lines of sight in the midplane. These two views were the ones available for the installation of the multichord MSE system on MAST.

The upper graph of Fig. 4 reveals a better spatial resolution for the top view. However, the improved spatial resolution of the top view is overshadowed by the larger $d\gamma/d\lambda$—and hence the larger sensitivity toward systematic errors—and the lower polarization fraction and normalized S/N ratio compared to the midplane view (see middle and lower graphs of Fig. 4).

The lower $p_l$ for the top view can be explained by the fact that the emission direction is more aligned with the electric field for typical MAST plasmas (with antiparallel $B_\phi$ and

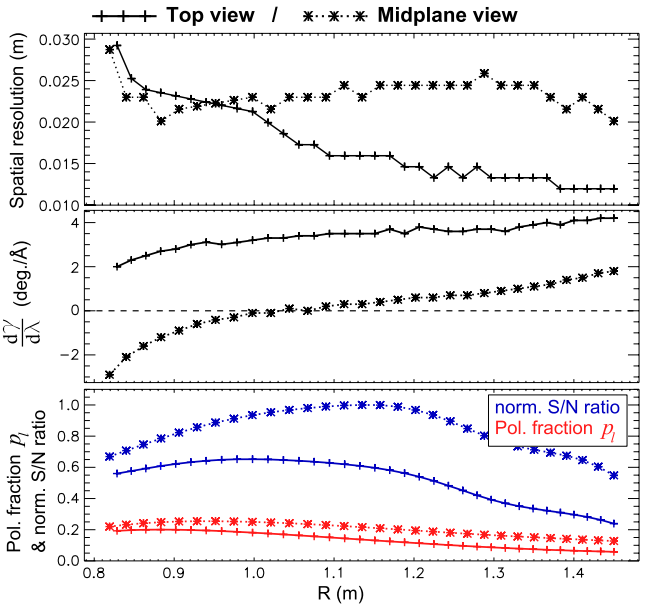


FIG. 4. (Color online) Spatial resolution, $d\gamma/d\lambda$, $p_l$ and normalized $S/N$ ratio for a top viewing geometry and for a viewing geometry in the midplane.

plasma current $I_p$). The higher $d\gamma/d\lambda$ can be attributed to the larger asymmetry in the vertical angles of the beam velocity distribution with respect to the lines of sight, compared to the midplane view. A view from below the midplane would be better from a polarization fraction point of view, but the asymmetry in the vertical velocity distribution angles would be equally bad as in the top view.

One can modify the fiber bundle layout to bring the spatial resolution of the top view up to the value of the midplane view. This does result in an improvement of the S/N ratio (because the total signal increases), but the level of the midplane view is not reached and $d\gamma/d\lambda$ remains poor. These simulations clearly favored the midplane geometry over the top view.

Similar to the viewing geometry one can also run simulations with different settings for the interference filter bandwidth. The main result is a decrease in $d\gamma/d\lambda$, which is desirable, and a decrease in $p_l$ and S/N ratio, which is undesirable, with increasing bandwidth. The code predicted best performance for a bandwidth of about 1.2 Å.

## IV. MULTICHORD MSE SYSTEM ON MAST

The MSE spectrum modeling code was used as a tool in the design of the multichord MSE diagnostic for MAST. The diagnostic has recently been installed and commissioning has started. A schematic of the diagnostic is given in Fig. 5.

The basic components of the multichord system are similar to those of the pilot diagnostic:[2] a dual photo elastic modulator (PEM) system that encodes the polarization state of the collected light into an intensity modulation,[12] 35 spatial channels, represented by a bundle of 19 fibers each, covering a range from $R=0.78$ m to $R=1.50$ m, and 42 filterscopes, containing a thin film interference filter and an avalanche photodiode (APD) detector.

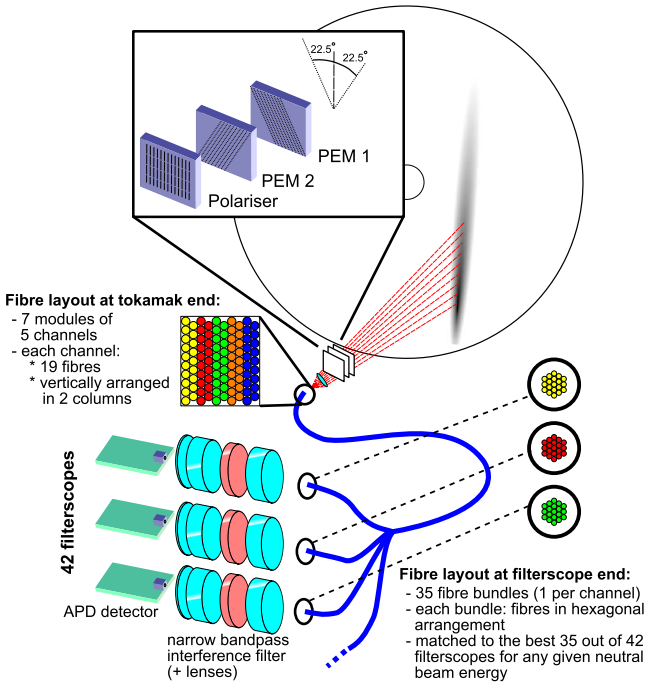


FIG. 5. (Color online) Overview of the multichord MSE setup at MAST.

Based on the better performance predicted by the simulation code, the collection optics were installed on a midplane diagnostic port of MAST. This in contrast to the top view used in the pilot system.

The narrow bandpass filters for selecting the $\pi$ or $\sigma$ component of the spectrum have a bandwidth of 1.2 Å FWHM—chosen based upon the MSE code—and a roughly Lorentzian band shape. The energy of the neutral beam determines the $\lambda_{CWL}$ of the filter for each channel. Because the beam energy can be varied over a range from $\approx$65 to $\approx$75 keV, a set of 42 filters is present. For any given beam energy the best matching 35 filters out of 42 are selected. A possible future upgrade using thermal tuning of $\lambda_{CWL}$ is under investigation.

Digital lock-in methods are applied to the APD signals, to extract the amplitudes of the harmonics of the PEM modulation frequencies (20 and 23 kHz). From these the Stokes vector of the detected light can be reconstructed.[12]

## V. SUMMARY AND OUTLOOK

The full MSE spectrum—$I(\lambda_{CWL})$, $\gamma(\lambda_{CWL})$, and $p_l(\lambda_{CWL})$—was simulated for the MAST tokamak. The code predicts a dependence of $\gamma$ on $\lambda_{CWL}$ and a low but acceptable $p_l$. The first can be a source of systematic errors (when $\lambda_{CWL}$ is imperfectly matched to the Stark spectrum) and the latter is proportional to the S/N ratio.

The simulation code was used within the design phase of the multichord MSE diagnostic on MAST and was a key tool in selecting the viewing geometry and the interference filter bandwidth.

The multichord MSE system is now installed. The MSE simulation code will be used during the commissioning of the diagnostic; identifying possible systematic errors, comparing calibration experiments with code simulations, providing MSE constraints to equilibrium reconstruction, and inclusion in Bayesian techniques for integrated data analysis.

## ACKNOWLEDGMENTS

This work was funded jointly by the UK Engineering and Physical Sciences Research Council and EURATOM.

[1] F. M. Levinton, R. J. Fonck, G. M. Gammel, R. Kaita, H. W. Kugel, E. T. Powell, and D. W. Roberts, Phys. Rev. Lett. **63**, 2060 (1989).
[2] M. Kuldkepp, M. J. Walsh, P. G. Carolan, N. J. Conway, N. C. Hawkes, J. McCone, E. Rachlew, and G. Wearing, Rev. Sci. Instrum. **77**, 10E905 (2006).
[3] H. Y. Yuh, Ph.D. thesis, Massachusetts Institute of Technology, 2005.
[4] M. F. Gu, C. T. Holtcomb, R. J. Jayakuma, and S. L. Allen, J. Phys. B **41**, 095701 (2008).
[5] H. Y. Yuh, F. M. Levinton, S. D. Scott, J. Ko, and W. A. Schumaker, Proceedings of the HTPD Conference, Albuquerque, 2008 (unpublished), Paper N23.
[6] S. A. Arshad, J. G. Cordey, D. C. McDonald, J. Farthing, E. Joffrin, M. von Hellermann, M. Roach, and J. Svensson, Fusion Sci. Technol. **53**, 667 (2008).
[7] P. G. Carolan, Proceedings of the 16th EPS Conference on Plasma Physics and Controlled Fusion, 1989 (unpublished), p. 1569.
[8] M. Turnyanskiy, Ph.D. thesis, University of Essex, 1999.
[9] L. C. Appel, G. T. A. Huysmans, L. L. Lao, P. J. McCarthy, D. G. Muir, E. R. Solano, J. Storrs, D. Taylor, and W. Zwingmann, contributors to the EFDA, Integrated Tokamak Modelling (ITM), Task Force, and JET-EFDA, Proceedings of the 33rd EPS Conference on Plasma Physics and Controlled Fusion, 2006 (unpublished), Paper No. EFDAJETCP(06)03-07, p. 2.184 (http://www.iop.org/Jet/fulltext/EFDC060307.pdf).
[10] S. J. Gee, R. Baldwin, A. Borthwick, D. Ciric, G. Crawford, L. Hackett, D. Homfray, D. Martin, J. Milnes, T. Mutters, M. Simmonds, R. Smith, R. Stephen, P. Stevenson, E. Surrey, C. Waldon, S. Warder, A. Whitehead, and D. Young, Fusion Eng. Des. **74**, 403 (2005).
[11] H. P. Summers, The ADAS User Manual, v2.6, 2004 (http://adas.phys.strath.ac.uk).
[12] M. Kuldkepp, N. C. Hawkes, E. Rachlew, and B. Schunke, Appl. Opt. **44**, 5899 (2005).